Liquid Crystals
Publication details, including instructions for authors and subscription information:
http://www.informaworld.com/smpp/title~content=t713926090

Thermopermeation in bicontinuous lyotropic crystals

P. Pieranski[a]
[a] Laboratoire de Physique, Université Paris-Sud, Orsay, France

First published on: 14 August 2009

To cite this Article Pieranski, P.(2009) 'Thermopermeation in bicontinuous lyotropic crystals', Liquid Crystals, 36: 10, 1049 — 1069, First published on: 14 August 2009 (iFirst)
To link to this Article: DOI: 10.1080/02678290902775216
URL: http://dx.doi.org/10.1080/02678290902775216

Liquid Crystals,
Vol. 36, Nos. 10–11, October–November 2009, 1049–1069

Taylor & Francis
Taylor & Francis Group

INVITED ARTICLE

Thermopermeation in bicontinuous lyotropic crystals

P. Pieranski*

Laboratoire de Physique, Université Paris-Sud, Bâtiment 510, 91405 Orsay, France

(Received 22 December 2008; final form 19 January 2009)

In 1982, P. G. de Gennes wrote two articles on two apparently disjoined subjects: (1) the Ludwig–Soret effect in porous media filled with pure liquids and (2) bicontinuous structures in microemulsions. In the study of bicontinuous cubic lyotropic crystals subjected to temperature gradients which we present here, these two subjects are now intimately related. Our experiments consist of the observation, by means of an optical microscope, of crystal shapes in three types of phase coexistence: Ia3d-in-vapour, Pn3m-in-L1 and Im3m-in-L1. In all three cases, we infer from changes in the crystal shapes that the surfactant is transferred, along the unique periodic bilayer, from the warm to the cold extremities of crystals. In order to explain this phenomenon of 'thermopermeation' of the surfactant, inspired by de Gennes we assume that: (1) the periodic bilayer acts as a viscoelastic matrix and (2) a slip occurs at the surfactant/water interface.

Keywords: Ludwig–Soret effect; bicontinuous lyotropic crystals; crystal shapes

1. Introduction

Of the 522 papers from the overwhelming legacy of de Gennes, 'only' 56 are devoted explicitly to liquid crystals and most of them were written in the early 1970s. The remaining 466 are distributed in other fields of condensed matter physics (magnetism, superconductivity, polymers, wetting, adhesion, granular systems, etc.) and in biology, the ultimate passion of de Gennes' scientific life. Knowing these facts, one understands better why most of de Gennes' contributions to the physics of liquid crystals were so crucial; such a universal encyclopaedic mind was able to shed new light on the 'beautiful and mysterious' phenomena occurring in liquid crystals.

The work presented here is related to two papers of de Gennes written in 1982 (see Figure 1). The first was a short condensed note on the Ludwig–Soret effect in a porous solid filled with a pure liquid (*1*). The second paper (*2*), which was much more extensive, dealt with bicontinuous structures (microemulsions) in oil/water/surfactant ternary mixtures and its main goal was to understand why such structures exist. Here, we show that shapes of monocrystals of cubic lyotropic phases, which also have bicontinuous structures, change drastically in temperature gradients. In order to interpret this new out-of-equilibrium phenomenon, we consider bicontinuous cubic crystals as porous media filled with water in which the Ludwig–Soret effect, as discussed by de Gennes, occurs.

This paper is organised as follows. First, we briefly review the two topics considered by de Gennes: the Ludwig–Soret effect and bicontinuous structures in lyotropic liquid crystals. Subsequently, we report on recent experiments with lyotropic cubic phases subjected to temperature gradients. In the last section, we show how to interpret our results in terms of de Gennes' theory.

1.1 Ludwig–Soret effect

1.1.1 Definitions

We know from the review paper of Platten and Costesèque (*3*) that the genuine Ludwig–Soret effect was discovered first by C. Ludwig in 1856 and confirmed 24 years later by Charles Soret. In a typical experiment, an aqueous salt solutions is held in a U-tube whose two extremities are subjected to different temperatures. Soret pointed out that the experimentally observed tendency of salts to concentrate at the colder extremity of the U-tube could not be explained in terms of Fick's law of diffusion alone and proposed to modify it by adding a second term proportional to the temperature gradient. Today, the Fick–Soret law for a binary mixture can be written as

$$\mathbf{j}_1 = -D(\rho\nabla w_1 + \rho w_1(1-w_1)S_T\nabla T), \qquad (1)$$

where $\mathbf{j}_1$ is the mass flux of the solute, w_1 its mass concentration, ρ is the density of the mixture, D is the diffusion coefficient and S_T the Soret coefficient. The product $DS_T = D_T$ is also known as the thermal diffusion coefficient. In the steady state defined by $\mathbf{j}_1 = 0$,

*Email: pieranski@lps.u-psud.fr

ISSN 0267-8292 print/ISSN 1366-5855 online

DOI: 10.1080/02678290902775216
http://www.informaworld.com

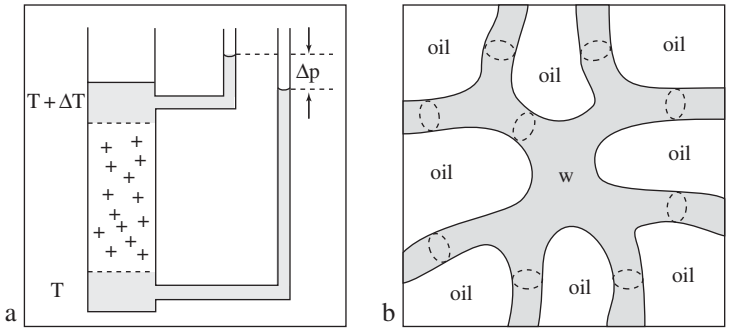

Figure 1. Genesis of the present work: (a) schematic of a system for measuring the intrinsic Soret effect in porous media (reproduced with permission from (*1*)); (b) 'cartoon' of the bicontinuous structure of microemulsions in ternary water/surfactant/oil systems; a network of interconnected oil tubes in a water matrix (reproduced with permission from (*2*)).

where diffusion and thermal diffusion are balanced, one has

$$S_T = -\frac{1}{w_1(1-w_1)}\frac{(\nabla w_1)_{st}}{(\nabla T)_{st}}. \qquad (2)$$

Following the terminology proposed by Figueiredo Neto (*4*, *5*), who studied the Ludwig–Soret effect in ferrofluids:

- when $S_T < 0$, the solute is said to be *thermophilic*, in a given solvent, because it concentrates in the hottest region;
- in the contrary case of $S_T > 0$, it is said to be *thermophobic*.

1.1.2 Experimental facts

Since its discovery, The Ludwig–Soret effect and its variants (thermophoresis, thermoosmosis) have been observed and measured by several more accurate and more rapid methods in many systems. Let us quote a few of them.

- *Solutions of organic compounds*. Wittko and Köhler (*6*) used a transient holographic technique (thermal-diffusion forced Rayleigh scattering, TDFRS) to measure the diffusion and thermal diffusion coefficients of several organic compounds of small molecular mass dissolved in protonated and deuterated cyclohexane. They have shown, among other things, that the sign of the Soret effect is opposite, for example, for acetone in cyclohexane ($D_T \approx -10^{-7}$ cm^2 K^{-1} s^{-1}) and for dibromohexane in cyclohexane ($D_T \approx +10^{-8}$ cm^2 K^{-1} s^{-1}). The influence of the isotopic substitution has also been found. Knowing that the diffusion coefficient $D \approx 10^{-5}$cm^2 s^{-1}, one obtains $S_T \approx -10^{-2}$ K^{-1} and $S_T \approx +10^{-3}$ K^{-1}, respectively.
- *Aqueous solutions of biopolymers and ionic surfactants*. A laser-beam deflection technique was used by Giglio and Vendramini (*7*) for the determination of the thermal diffusion coefficient in aqueous solutions of surfactants (SDS, Triton X-100) and biomolecules (lysozyme, bovine serum albumin). In particular, they have found that SDS displays the thermophobic behaviour ($S_T > 0$). The same technique was used later by Piazza and Guarino (*8*) who measured the Soret coefficient S_T in the micellar phase of SDS/water solutions as a function of the surfactant concentration and of the ionic strength. The most important outcome of these experiments was that the Soret coefficient grows when $w \to 0$. This effect is increasingly pronounced when the ionic strength decreases so that the Soret coefficient can be as large as $S_T \approx 0.2$ K^{-1}.
- *Aqueous solutions of non-ionic surfactants*. In the context of the present paper, the work of Ning *et al.* (*9*) is the most meaningful as it was performed with solutions of non-ionic surfactants C_mEO_n in water. Using the TDFRS technique, Ning *et al.* have found that at low concentrations, i.e. in the micellar isotropic phase L1, these surfactants display the thermophobic behaviour and that the value of the Soret coefficient varies from $S_T \approx 0.01$ K^{-1} to $S_T \approx 0.3$ K^{-1} as a function of concentration and temperature.

1.1.3 Ludwig–Soret effect driven by the surface slip: thermophoresis

The abnormally large values of the Soret coefficient in micellar solutions of surfactants can be explained in terms of *thermophoresis (10, 11)* involving the *surface slip mechanism* proposed by Ruckenstein (*12*) and quoted by de Gennes in his note (*1*).

The surface slip consists of a tangential discontinuity of the velocity field at the solid/liquid interface.

In the reference frame of the solid, the slip velocity is proportional to the component of the temperature gradient parallel to the surface:

$$\mathbf{v}_{\text{slip}} = -D_{\text{slip}} \nabla_{\parallel} T. \tag{3}$$

Würger (*11*) has shown recently that in the case of a spherical particle of radius a suspended in a fluid, this surface slip, induced by the temperature gradient, generates the velocity field shown in Figure 2(a). In spherical coordinates (r, θ), it is given by

$$\mathbf{v}(\mathbf{r}) = u \frac{a^3}{r^3} \left(\frac{1}{2} \sin\theta \mathbf{t} + \cos\theta \mathbf{n} \right). \tag{4}$$

This field has several remarkable features:

- the particle drifts in the x direction with velocity $\mathbf{u} = u\mathbf{e}_x$;
- at $(a, \pi/2)$, the fluid flows in the opposite direction with velocity $-u/2$;
- the resulting slip velocity, calculated at $(a, \pi/2)$, is $v_s = -3u/2$;
- the integrated flux of the fluid through the plane $\theta = \pi/2$ is $-\pi a^2 u \mathbf{e}_x$;
- for $r > a$, the orientational average of the flow velocity on the whole solid angle 4π vanishes.

This last property has an important consequence: in a suspension of a finite concentration, hydrodynamic interactions with other particles average to zero so that all particles drift with the same mean velocity $\mathbf{u} = u\mathbf{e}_x$. In other words, thermophoresis is not affected by hydrodynamic interactions.

1.1.4 Ludwig–Soret effect driven by the surface slip: thermopermeation

When a porous solid matrix is filled with a fluid and the surface slip, driven by a temperature gradient, occurs at the surfaces of the channels, then the fluid will flow through the matrix. This variant of the Ludwig–Soret effect can be called thermopermeation.

A suspension of spherical particles having some fixed configuration in space can be seen as a peculiar example of a porous material. From considerations in the previous section we have the result that when such a set of particles is kept at rest in the laboratory frame, then upon the action of a thermal gradient, the fluid will flow through it with the average velocity $u = (2/3)v_{\text{slip}}$ where v_{slip} is the slip velocity given by (3).

In (*1*), de Gennes discusses another type of porous material made of a solid matrix containing channels, of axial symmetry, parallel to the direction $\mathbf{e}_x$ of the temperature gradient (see Figure 2(b)). When the local radius $R(x)$ is constant, then the flow is of the plug type, with velocity v_{slip}. However, when $R(x)$ varies with x (see Figure 2(b)), some local pressure gradients along the channel are necessary to maintain the constant total flux J through sections with variable surface area $\pi R(x)^2$ and one has

$$J = \pi R^2 \left(v_{\text{slip}} - \frac{R^2}{32\eta} \nabla p \right). \tag{5}$$

In the example shown in Figure 2(b), these pressure gradients generate *reverse flows* in the channel's segment with the large section but have little effect on the plug flow profile in narrow sections. With the condition that there is no pressure difference between extremities of such a corrugated channel

$$\int \nabla p = 0, \tag{6}$$

de Gennes obtained

$$J = v_{\text{slip}} \pi \frac{\langle R^{-2} \rangle}{\langle R^{-4} \rangle}, \tag{7}$$

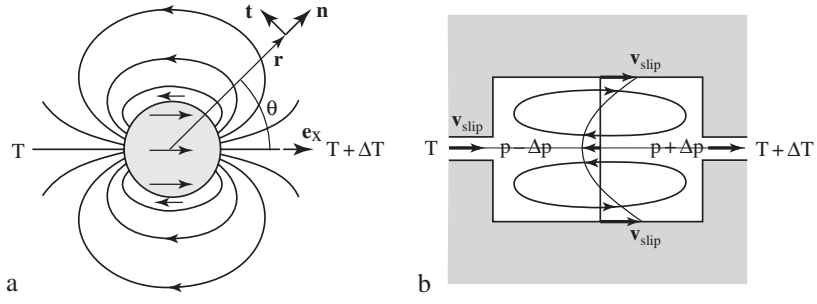

Figure 2. Ludwig–Soret effects driven by the surface slip. (a) Thermophoresis: drift of a colloidal particle (e.g. a surfactant micelle) in the solvent due to the surface slip (following Würger (*11*)). (b) Thermopermeation: flow of fluid due to the slip on the surface of a channel in a porous solid (following de Gennes (*1*)).

where $\langle \ldots \rangle$ is the average along x. As a result, for a given slip velocity, the effective flux is mostly limited by narrow sections of channels.

1.2 Bicontinuous lyotropic phases

In the present paper we report on Ludwig–Soret experiments performed with a third, very peculiar type of porous material: bicontinuous lyotropic phases. The concept of bicontinuous structures in lyotropic systems has at least two different roots: microemulsions and cubic phases.

1.2.1 Microemulsions in water / surfactant / oil ternary systems

The schematic representation of microemulsions, used explicitly by de Gennes and Taupin (*2*) and shown here in Figure 1(b), is based on the work of Scriven who stated clearly the concept of bicontinuous structures for the first time in 1977 in these terms (*13*):

> 'What are the ways of filling the space with two material phases, or with two compositions of matter? Conventional thinking about fluid phases is that one or the other forms a continuum in which the second phase is dispersed as discrete globules or as less symmetric blobs. Water/oil emulsions are supposed to be either water-continuous or oil-continuous. For microemulsions, micellar solutions, mesomorphous phases and certain lyotropic liquid crystalline phases the possibilities are held to be blobs of one composition dispersed in another, or tubules of one threading the other, or lamella of one alternating with the other. Among common solid/fluid interspersions are examples of another possibility: *both* phases continuous as in sandstone, fritted glass, sponge and many other porous materials.'

It is interesting to note that as an example of such a bicontinuous structure, Scriven quotes the partition of space by the triply periodic minimal surface of symmetry Im3m, invented by Schwarz, represented here in Figure 3(a). In order to model microemulsions which are not periodic, Scriven considers the possibility of

> 'a bicontinuous structure that is not periodic but topologically equivalent to one that is; i.e. the two may be related by a continuous transformation that destroys symmetry but preserves genus.'

It has been pointed out later by Teubner (*14*) that isosurfaces of Gaussian random fields (see Figure 3(b)) have all of the features of surfaces imagined by Scriven.

1.2.2 Bicontinuous cubic phases in surfactant/water binary mixtures

The concept of bicontinuous structures also appeared in the context of structural studies of surfactant/water binary mixtures. In a historical perspective sketched in the first chapter of a recent book devoted to bicontinuous liquid crystals (*15*), Larsson stresses the importance of the work of Luzzati *et al.* (*16*) on lipid/water systems.

Indeed, the model of symmetry Ia3d for anhydrous strontium myristate proposed by Luzzati *et al.* is bicontinuous: two interwoven scaffoldings made of surfactant. Stimulated by Luzzati *et al.*, Larsson *et al.* (*17*) performed X-ray and nuclear magnetic

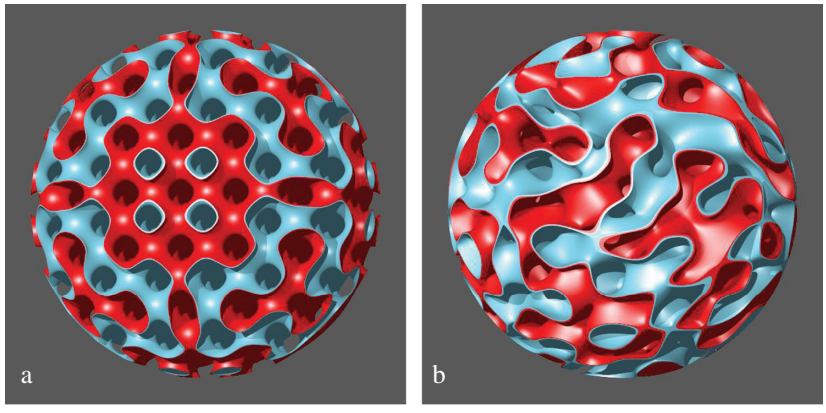

Figure 3. Scriven's models of microemulsions: bicontinuous structures resulting from the partition of space by high-genus surfaces. The bright and dark labyrinths are filled respectively with water and oil and are separated by a monolayer of surfactant. (a) Structure of Im3m symmetry based on a triply periodic isosurface similar to the Schwarz's minimal surface. (b) Disordered structure generated by an isosurface of a Gaussian random field. In water/surfactant binary mixtures where both labyrinths are filled with water, these models correspond to: (a) the cubic Im3m phase and (b) the sponge phase.

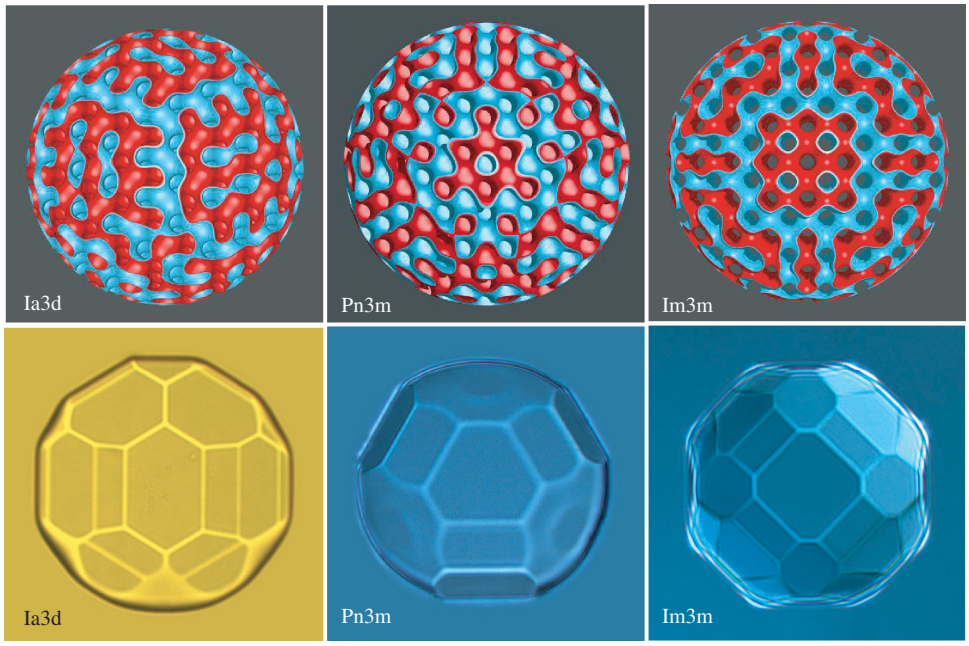

Figure 4. Bicontinuous cubic lyotropic phases. Pictures of level surfaces in the upper row illustrate the shapes of the surfactant bilayer. Pictures in the lower row are images of real crystals observed in a transmission optical microscope. Ia3d, monocrystal of the Ia3d phase of monooelin grown using a hygroscopic technique. Pn3m, monocrystal of the Pn3m phase of phytantriol grown using a isoplethal technique with an excess of water. Im3m, monocrystal of the Im3m phase in a phytantriol/water/ethanol mixture.

resonance (NMR) studies of monoolein/water binary mixtures. Initially, it seemed that one cubic phase of symmetry Im3m occurs in this system. However, further works of Longley and McIntosh (*18*), Hyde *et al.* (19) and Qiu and Caffrey (*20*) lead to the conclusion that not one but two bicontinuous cubic phases exist in the monoolein/water system and that their symmetries are Pn3m and Ia3d. More precisely, the phase of symmetry Pn3m is obtained with an excess of water. At lower water contents, it transforms into the Ia3d phase. Later, it has been shown that about 3% of distearoylphosphatidylglycerol added to the monoolein induces the Pn3m-Im3m phase transition (*21*). Recently, a very similar polymorphism has been observed with phytantriol (*22*, *23*). The same bicontinuous cubic phases have also been found in aqueous solutions of other surfactants. An excellent review on this subject has been written by Fontell (*24*). In our studies of the Ludwig–Soret effect, in addition to the monoolein and phytantriol, non-ionic surfactants $C_{12}EO_2$ and $C_{12}EO_6$ have also been used.

In conclusion, in all three cubic phases of these materials, the surfactant is assembled into a bilayer which is liquid in its two dimensions and which separates two interwoven water channels. The shapes of this unique, continuous bilayer are periodic in three dimensions, i.e. invariant with respect to operations of the corresponding space groups Ia3d, Pn3m and Im3m. Analytically, these shapes can be approximated either by triply periodic minimal surfaces (TPMS) or by level surfaces (LS) of suitable symmetry (see, e.g., (*25*)). The LS representation is more convenient in practice and we used it for the drawings shown in the upper row of Figure 4.

1.3 Isothermal shapes of Ia3d, Pn3m and Im3m crystals

In all of the studies mentioned above, the cubic structures Ia3d, Pn3m and Im3m were inferred from X-ray diffraction diagrams. The use of X-rays can be avoided when it is possible to grow monocrystals and observe their shapes. Indeed, it has been well known since the beginnings of crystallography that the crystal habits of solid crystals are related to their structure. The basics of this empirical method of identification of crystal symmetries are outlined in, for example, the books of Friedel (*26*) or Phillips (*27*).

1.3.1 Typical isothermal shapes observed in experiments

In lyotropic systems, the first observations of the shapes of cubic crystals were made by Winsor (*28*) and Sotta (*29*). Subsequently, new special methods called *hygroscopic* and *isoplethal* were developed with

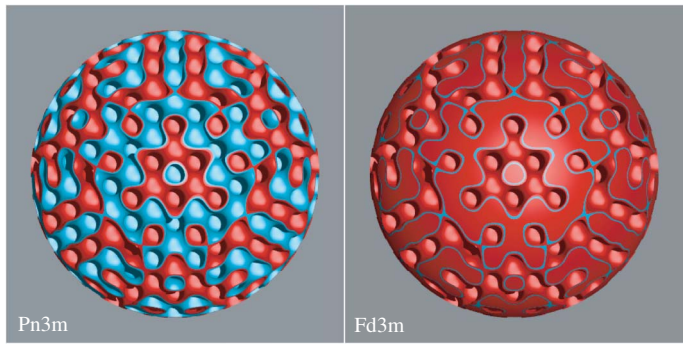

Figure 5. Topological symmetry breakdown. Pn3m: Occurrence of prohibited bilayer's edges on the surface of a Pn3m crystal. Both water labyrinths communicate with the L1 phase surrounding the crystal. Fd3m: Surgery of its bilayer restores the integrity. As a result, one of the water labyrinths is 'imprisoned' inside the bilayer.

the aim of performing controlled growth of monocrystals of cubic lyotropic phases and to observe their shapes by means of an optical microscope (for a review, see (*30*)). A few technical details about these methods are given in the next section. By way of an introduction, let us just say that the observed shapes of the Ia3d, Pn3m and Im3m monocrystals are so characteristic that a univocal relationship between crystal shapes and structures can be established. This is illustrated by three typical pictures shown in the lower row of Figure 4 and can be summarised as follows.

- *Ia3d crystals* are grown using a hygroscopic method from L2 droplets surrounded by a humid atmosphere (*31*, *32*). Most frequently, they are oriented with (211) planes parallel to glass or mica substrates. On their Ia3d/vapour interface, the most prominent facets are (112), (220), (321), (400) and (420).
- *Pn3m crystals* are grown from L2-in-L1 droplets (*33*). Typically, they are oriented with (111) planes parallel to glass surfaces. On their Pn3m/L1 interface, the most prominent facets are (111), (220), (400), (311) and (331).
- *Im3m crystals* are grown from L2-in-L1 droplets. Their spontaneous orientation is (100)//glass. On their Im3m/L1 interface, the most prominent facets are (100), (111), (110) and (211).

1.3.2 Topological symmetry breakdown

The series of the most prominent facets observed on the Ia3d/vapour interface corresponds, as expected, to the Donnay–Harker empirical rules of classical crystallography. Remarkably, this is not the case for Pn3m/L1 and Im3m/L1 interfaces. Indeed, in terms of the Donnay–Harker rules, the observed series of the most prominent facets would rather correspond, respectively, to Fd3m and Pm3m symmetries. This apparent disagreement between experiments and theory unveils an important topological constraint in bicontinuous lyotropic structures: the prohibition of the bilayer's edges. In order to satisfy this constraint and to restore the integrity of the bilayer, surgery must be performed at the Pn3m/L1 and Im3m/L1 interfaces. After the surgery, one of the two water labyrinths is 'imprisoned' inside the bilayer as shown in Figure 5. As a result, the equivalence of the two labyrinths is broken so that symmetry breakdowns Pn3m → Fd3m and Im3m → Pm3m occur at least as far as faceting is concerned.

2. Crystal shapes in temperature gradients

After the above descriptions of bicontinuous cubic lyotropic phases it seems legitimate to consider them as 'porous media filled with water' in which the Ludwig–Soret effect discussed by de Gennes in his paper (*1*) is likely to occur. The generic idea of de Gennes has nevertheless to be transposed because the porous matrix made of surfactant is also liquid. In such a 'porous liquid medium', the thermal diffusion of water (or water/ethanol solution) with respect to the periodic matrix should be accompanied by the thermal diffusion, in the opposite direction, of the surfactant inside the bilayer. The aim of the experiments presented below is to detect the thermal diffusion of the surfactant from changes in the crystal shapes induced by temperature gradients. By crystal shapes we mean the shapes of interfaces between cubic phases and isotropic phases coexisting with them. In Figure 4, examples of Ia3d/vapour, Pn3m/L1 and Im3m/L1 interfaces were shown. The two remaining possible types of interfaces, cubic/L2 and cubic/sponge, are not considered here because they are not facetted.

2.1 Ia3d/vapour interface, $C_{12}EO_6$/water binary system

2.1.1 Setup for hygroscopic studies

As already mentioned above, Ia3d monocrystals (such as that shown in Figure 4) can be grown using a so-called hygroscopic method using, for example, the setup shown schematically in Figure 6. Its operating principle is as follows: the sample, a cubic Ia3d crystal on a mica sheet (or a glass plate) here, is in thermal contact with a copper plate whose temperature $T_s = T_1 = T_2$ is regulated precisely by means of two Peltier elements located on a thermalised aluminium base. As explained in (*32*), the water content of the sample depends on the partial pressure p of water vapours surrounding it, i.e. on the local humidity defined as

$$h = \frac{p}{p_s(T_s)} \cdot 100\%, \tag{8}$$

where $p_s(T_s)$ is the pressure of saturated vapour at temperature T_s. Now as water vapours are produced by the water reservoir located beneath the sample, they are saturated at temperature T_o of water so that $p = p_s(T_o)$ and

$$h = \frac{p_s(T_o)}{p_s(T_s)} \cdot 100\%. \tag{9}$$

2.1.2 Shapes of the Ia3d/vapour interface in temperature gradients

Using this setup, the phase diagram of temperature versus humidity of the monoolein shown in Figure 7

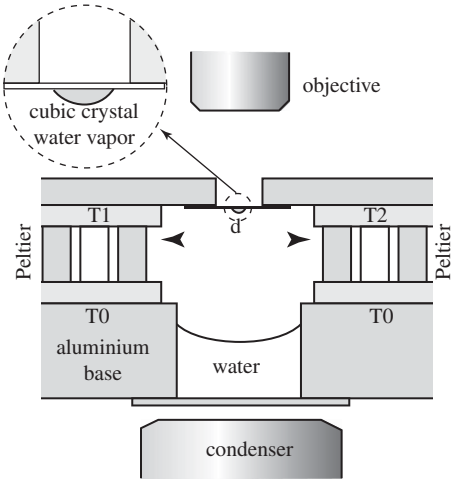

Figure 6. Experimental setup for hygroscopic studies. The sample, located on a mica sheet (or a glass plate), is surrounded by water vapours produced by a water reservoir. (Made in collaboration with C. Even, D. Rohe, L. Sittler, J. Grenier and S. Leroy.)

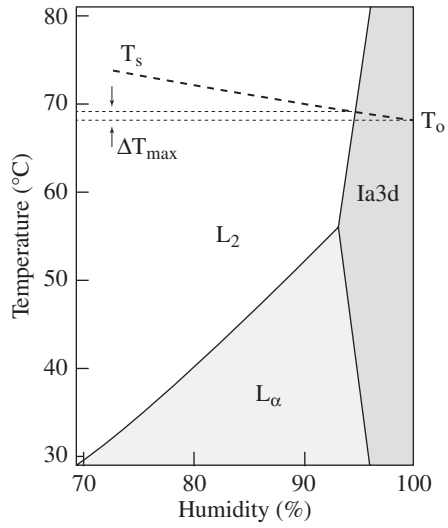

Figure 7. Phase diagram of the monoolein/water binary system established by means of the hygroscopic setup shown in Figure 6. (Made in collaboration with J. Okal and P. Faye.)

has been established. When the temperature of the water reservoir is set to T_o and the temperature of the sample T_s varies, the path along the dotted line T_oT_s is followed in this phase diagram. It is therefore possible to grow Ia3d crystals from the L2 phase. The Ia3d crystal shown in Figure 4 has been obtained using this method.

Now, in the hygroscopic setup shown in Figure 6, temperatures T_1 and T_2 can be regulated independently so that a horizontal temperature gradient can be created. With an appropriate choice of these temperatures (e.g. $T_1 < T_o < T_2$) the Ia3d phase can be preserved in spite of the temperature gradient. The typical width of crystals is about 0.1 mm. When $(T_1 - T_2)/d \approx 1$ K mm^{-1}, the temperature difference between left and right extremities of the crystal is 0.1 K, i.e. about 10 times less than ΔT_{max} in Figure 7. When such a horizontal temperature gradient is applied to an Ia3d crystal, its shape changes on the time scale of few hours as shown in Figure 8. Clearly, the crystal is growing on its colder side and is simultaneously deconstructed on its warmer side. During the entire process the amount of surfactant in the crystal is constant so that the surfactant is transferred from the warmer to the colder side of the crystal.

If one considers the Ia3d crystal as an organised surfactant/water solution, then the behaviour of the surfactant could be qualified as thermophobic in terms of the vocabulary of the Ludwig–Soret effect. However, the principle of the hygroscopic method is based on the variation of the saturated vapour pressure with temperature. Therefore, in the presence of a

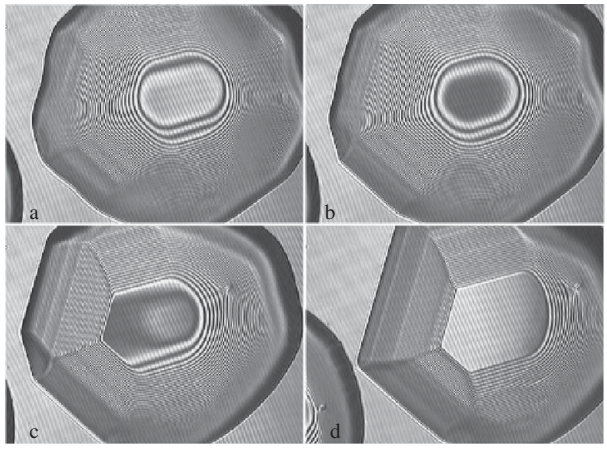

Figure 8. Evolution of the shape of an Ia3d crystal subjected to a temperature gradient. The crystal is colder on its left side.

temperature gradient, the relative humidity defined in (9) increases from the warmer to the colder side of the crystals. Thus, the observed behaviour of the surfactant could also be qualified as *hygrophilic*. We will see in the next section that this ambiguity is avoided in lyotropic systems with a solubility gap in which cubic phases can coexist with the L1 phase made of almost pure water.

2.2 *Pn3m-in-L1 crystals, $C_{12}EO_2$ binary system*

Among the large variety of lyotropic systems in which a solubility gap occurs, we chose to work with $C_{12}EO_2$, monoolein and phytantriol because we know these surfactants well from previous studies (*30*, *32–35*); in these three systems, the Pn3m bicontinuous phase is formed in an excess of water.

2.2.1 *Setup for isoplethal studies and preparation of samples*

Monocrystals of the Pn3m phase surrounded by the L1 phase were grown and observed by means of the setup shown schematically in Figure 9. The sample, a Pn3m monocrystal, is situated on the upper wall of a flat glass capillary of section 0.2×4 mm^2. The capillary is placed on two Peltier elements which are in thermal contact with a metallic base. The temperatures T_1 and T_2 are set independently with a precision of 0.01 K and the stability of the regulation is of the order of 0.001 K. The sample is observed in transmitted light. The distance d between Peltier elements can be adjusted. The capillary is pressed against Peltier elements using a plastic foam part not shown in this diagram. The role of this part is also to provide thermal insulation from above. When this part is removed, a vertical temperature gradient can be created.

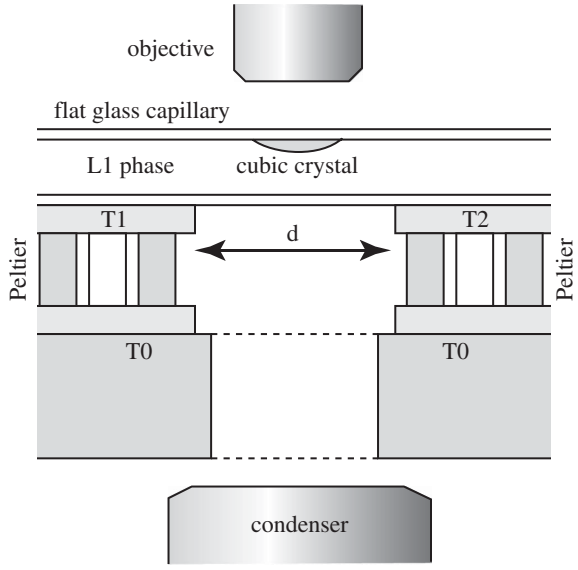

Figure 9. Experimental setup for isoplethal studies. The sample, situated on the wall of a flat glass capillary, is surrounded by the L1 phase. (Made in collaboration with M. Bouchih, N. Ginestet, S. Popa-Nita, T. Plötzing, J. Okal, P. Faye, R. Sheska, G. Saquet and J. Rizzi.)

One of the methods of preparation of the samples, i.e. Pn3m-in-L1 crystals, has been described in detail in (*33*). For example, in the case of $C_{12}EO_2$ surfactant, it starts by filling the flat capillary with an emulsion of the sponge phase L3 in the micellar phase L1 at room temperature. Under the action of the buoyancy force, small droplets of the sponge phase reach the upper wall of the capillary where they spread partially. These small droplets of the sponge phase are transformed into defectless monocrystals of the Pn3m phase through the two-stage path **1** + **2** in the phase diagram in Figure 10 established by Lynch *et al.* (*36*).

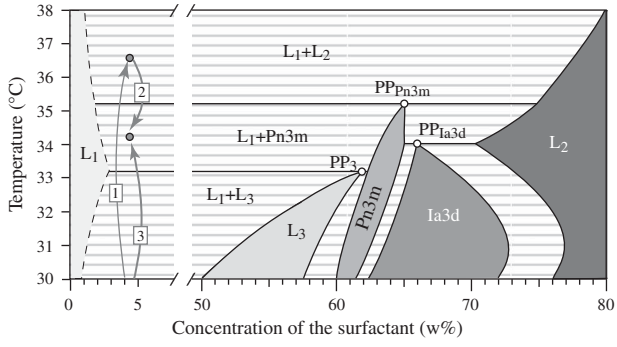

Figure 10. Phase diagram of the $C_{12}EO_2$/water mixture established by Lynch *et al.* (*36*). The limits of the micellar L1 phase drawn with dashed lines are hypothetical. Note the presence of three peritectic points corresponding to the upper temperature limits of the L3, Pn3m and Ia3d phases. Faceting occurs only in the domain of coexistence L1+Pn3m.

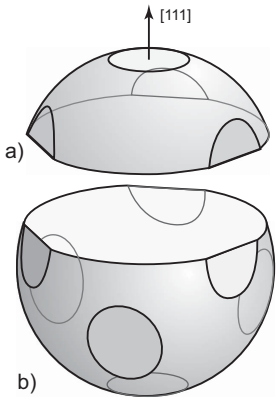

Figure 11. Perspective view of complementary concave and convex shapes of the Pn3m/L1 interface: (a) inclusion of the L1 phase inside a Pn3m crystal; (b) Pn3m crystal situated at the upper wall of the flat capillary and surrounded by the L1 phase. In experiments, such inclusions and crystals are observed from the direction of the [111] ternary axis.

Pn3m crystals obtained using this method are usually oriented with their (111) planes parallel to the capillary wall and, as shown in Figure 11(b), are always truncated because the contact angle between L1/Pn3m and glass/Pn3m interfaces is about 110°.

Large L3 drops introduced into the capillary are squeezed between its walls and have pancake-like shapes (see (*33*)). After the 1 + 2 path, these large drops are also transformed into Pn3m crystals with the (111) planes parallel to the capillary walls. In such large crystals, inclusions of the L1 phase are nucleated by another process described in (*33*). The typical shape of L1-in-Pn3m inclusions is depicted in Figure 11(a).

2.2.2 Deformation of Pn3m crystals in a temperature gradient parallel to the capillary walls, (111)//glass orientation

When a temperature gradient parallel to the longitudinal axis of the glass capillary is applied, one observes a progressive deformation of Pn3m crystals situated at the capillary walls. This is illustrated by the series of four photographs in Figure 12 which were taken at intervals of 1 hour (*37*). The temperature gradient applied here was grad $T = 0.6$ K mm^{-1}.

Clearly, upon the action of the temperature gradient, the facets located on the colder side of the crystal increase in size while those located on the warmer side are shrinking. The perspective views (Figure 12(a′)–(d′)) help to better visualise these gradient-induced changes in the crystal shape.

In order to quantify the changes in crystal shapes, videos of deforming crystals have been recorded at a typical rate of 1 frame per 100 seconds. In Figure 13 we show four frames selected at intervals of about 1 hour from such a video recorded with a gradient of 0.9 K mm^{-1}. More detailed information on the evolution of colder and warmer facets can be obtained by means of the 'reslicing' computer procedure (in the ImageJ software) which allows us to extract arbitrary spatiotemporal cross sections from this video. As an example, we show in Figure 14 the evolution along the line A crossing the warmer facet (defined in Figure 13(a)). The most interesting feature revealed by this spatiotemporal cross section is that the macroscopic steps are continuously nucleating, at the edge of the warmer facet, and collapsing in its centre.

Four spatiotemporal cross sections along the line B passing through the colder facet (defined in Figure 13(a)) are shown in Figure 15. The first cross

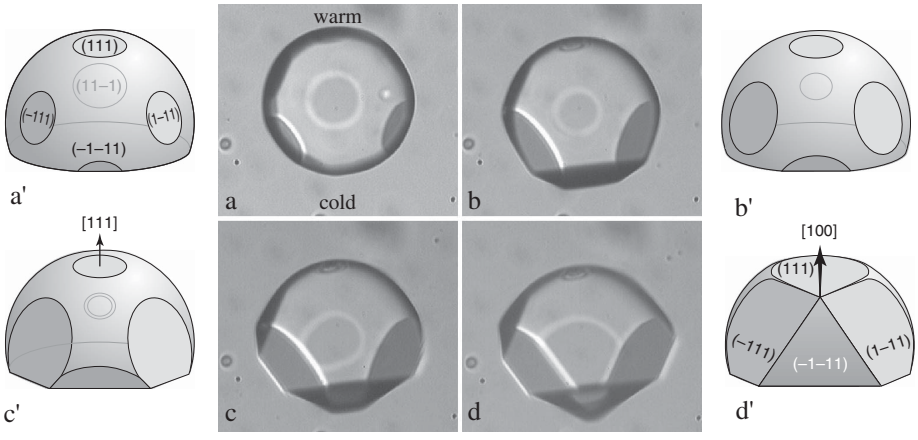

Figure 12. Deformation of a Pn3m-in-L1 crystal subjected to a temperature gradient parallel to the capillary wall. (a)–(d) Experiments with a $C_{12}EO_2$/water binary mixture. The temperature variation across the crystal is 0.05 K. The crystal is observed from the direction of the [111] axis. (Made in collaboration with S. Popa-Nita (*37*).) (a′)–(d′) Corresponding perspective views.

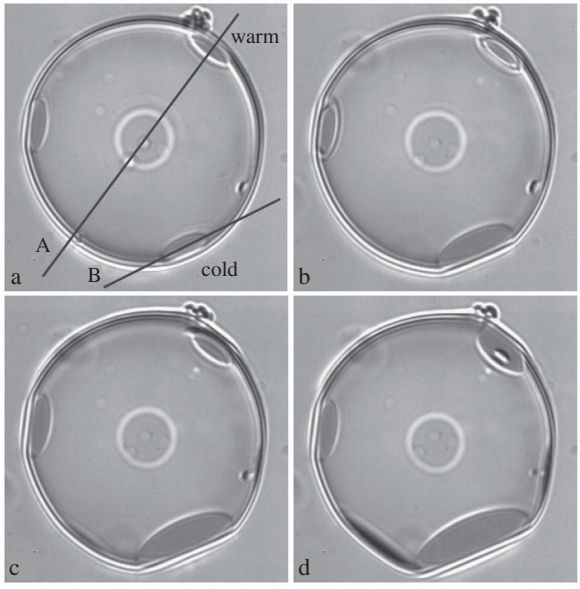

Figure 13. Four frames from a video of a Pn3m crystal deformed by a horizontal temperature gradient of 0.9 K mm^{-1}. On the warner facet one sees the formation and collapse of a macroscopic step. The evolution of the crystal along the line A over 3.5 hours is shown in Figure 14.

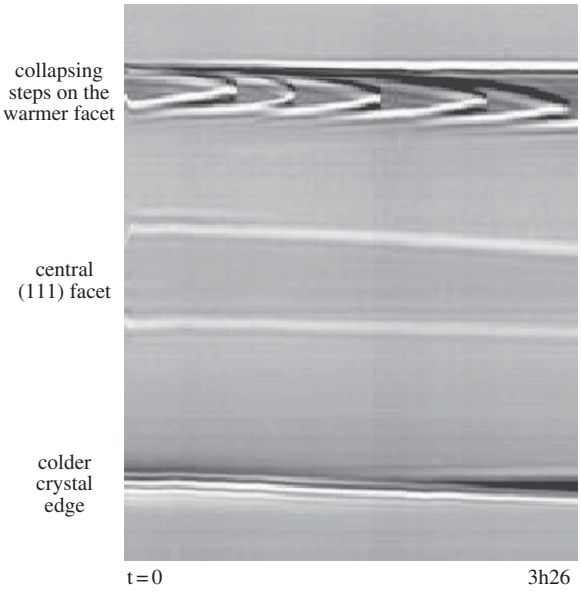

Figure 14. Spatiotemporal representation of the evolution of the crystal shown in Figure 13. For the reslicing procedure, the line A from Figure 13a has been selected. Note the periodic nucleation and collapse of macroscopic steps on the warmer facet. The central (111) facet keeps its size but is slightly shifted towards the colder side of the crystal.

section has been extracted from the video recorded with the temperature gradient of 0.9 K mm^{-1}. The other three have been obtained using the same crystal

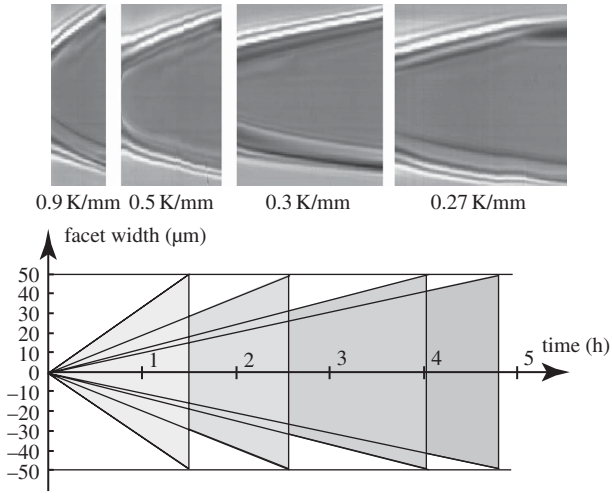

Figure 15. Spatiotemporal representations of the evolution of the crystal shown in Figure 13. For the reslicing procedure, the line B from Figure 13(a) has been selected. Clearly, the rate dD/dt at which the facet's diameter grows depends on the temperature gradient. In order to estimate the growth rate, a graphical method has been used.

with smaller values of the temperature gradient. Clearly, at the initial stage of the crystal evolution, the diameter D of the colder facet is growing and, in the first approximation, the variation $D(t)$ is linear. The growth rate dD/dt, determined graphically from each pattern, is plotted versus the temperature gradient in Figure 16. The plot of dD/dt versus ΔT fits well with a linear low.

At this stage of the study it became clear that processes occurring at warmer and colder sides of the crystal are similar to growth and melting of crystals. On the colder side, the apparent growth of the crystal

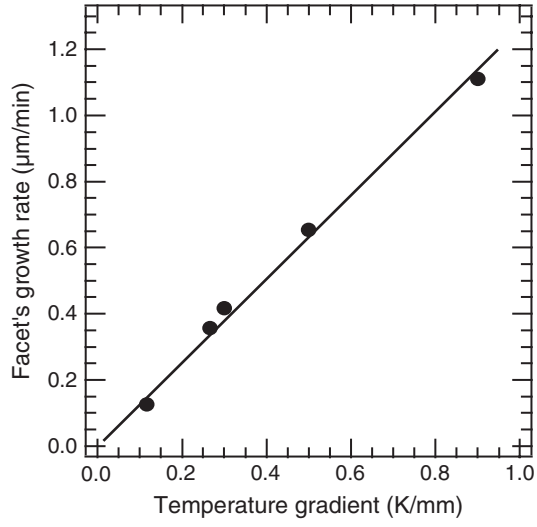

Figure 16. Growth rate of the colder facet diameter versus the temperature difference between the Peltier elements.

involves exclusively progression (an outward motion) of rough surfaces, the facets being blocked. The apparent 'melting' of the crystal on its warmer side is rather a kind of a 'deconstruction' process taking place both on rough surfaces and on facets. The rough surfaces are retroceding continuously while the motion of facets is mediated by the nucleation and collapsing of steps of a macroscopic height. Such macroscopic steps are visible on the warmer facet in Figure 13.

2.2.3 Deformation of Pn3m crystals in a temperature gradient parallel to the capillary walls, (110)//glass orientation

Similar changes in crystal shapes are induced by the horizontal temperature gradient in crystals having different orientations. For example, in Figure 17 we illustrate, using four pictures selected from a video, the evolution of a crystal oriented (approximatively) with (110) planes parallel to the wall of the glass capillary. The horizontal temperature gradient is (approximatively) parallel to the four-fold [100] axis. This peculiar (abnormal) orientation has several advantages:

- two facets (one colder and one warmer) make the same angle of 35° with the direction of observation so that they are well visible;
- their position with respect to the crystal centre is symmetrical;
- four other facets are parallel to the direction of observation.

Here, as for the common (111)//glass orientation discussed previously, the Pn3m crystal is also growing on its colder side and simultaneously is deconstructed on the warmer side. The spatiotemporal cross section extracted from the line A of the video and shown in Figure 18 provides detailed information on the behaviour of the slightly oblique facets. The diameter of the colder facet is growing, while on the warmer facet a periodic nucleation of macroscopic steps takes place. These steps collapse one after another in the facet's centre. The same spatiotemporal cross section A shows that the rough surfaces on the cold and warm extremities of the crystals are moving; the crystal is growing on its cold side and is retroceding on its warm side. Let us emphasise again that the growing cold facets do not move because they are blocked by a prohibitive barrier of step nucleation.

All of these experimental facts prove that in the presence of the horizontal temperature gradient, the surfactant molecules must be transported somehow from the warm to the cold side of the crystal. In Section 3 we argue that this transport takes place trough the bulk of the crystal but before that we complete the experimental section with a few complementary observations.

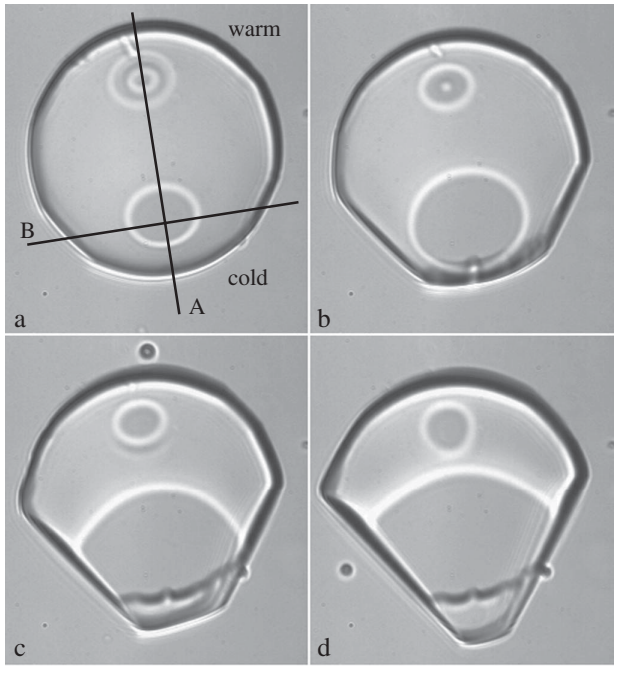

Figure 17. Deformation of a Pn3m crystal subjected to the horizontal temperature gradient. The picture (a) has been taken 8 minutes after the application of the temperature gradient of 1.33 K mm^{-1}. Three other pictures have been taken at 1 hour intervals.

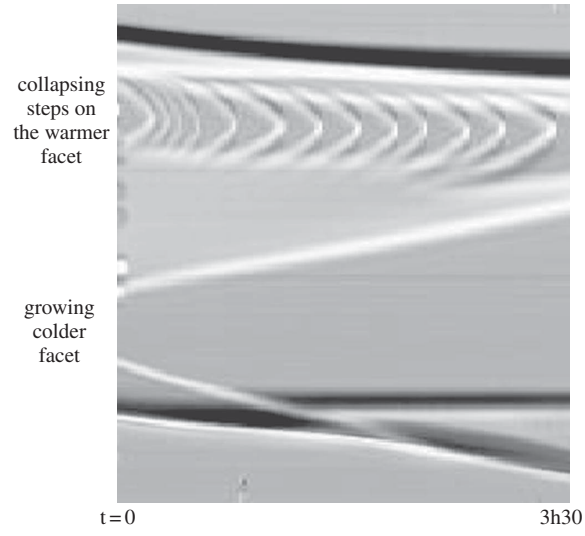

Figure 18. Spatiotemporal cross section showing the evolution of the crystal from Figure 17 along the line A. This pattern illustrates several features of the crystal shapes evolution: (1) the warmer (upper) extremity of the crystal is retroceding; (2) on its colder (lower) side the crystal is growing; (3) on the warmer facet one sees a periodic nucleation of macroscopic steps collapsing in the facet's centre; (4) the diameter of the colder facet is growing.

2.2.4 Pn3m-in-L1 crystals in a vertical temperature gradient

Even if the experimental setup shown in Figure 9 is not well adapted for this purpose, a few observations have also been made with a vertical temperature gradient applied to Pn3m crystals. In order to create such a gradient, the plastic foam part, providing the thermal insulation of the sample from the top, has been removed. In this configuration, the upper wall of flat capillary (see Figure 9) becomes slightly cooler than the bottom wall. We know already that Pn3m crystals are usually located at the upper wall of the capillary and their threefold [111] axis is orthogonal to it (see Figure 11).

In this configuration, the vertical temperature gradient is parallel to this [111] axis so that one expects that the threefold symmetry of the crystal should be preserved. Figure 19(b) proves that this is actually the case. On the other hand, the relative extensions of the (111)-type facets should now depend on their vertical position z. By analogy with the case of the horizontal gradient it is expected that the facets on the upper, colder side of the crystal should increase in diameter while those on the lower warmer side should shrink. This is effectively the case in Figure 19(b). The perspective views in Figure 19(a′) and (b′) help to visualise the positions of the facets with respect to the capillary wall and to the gradient.

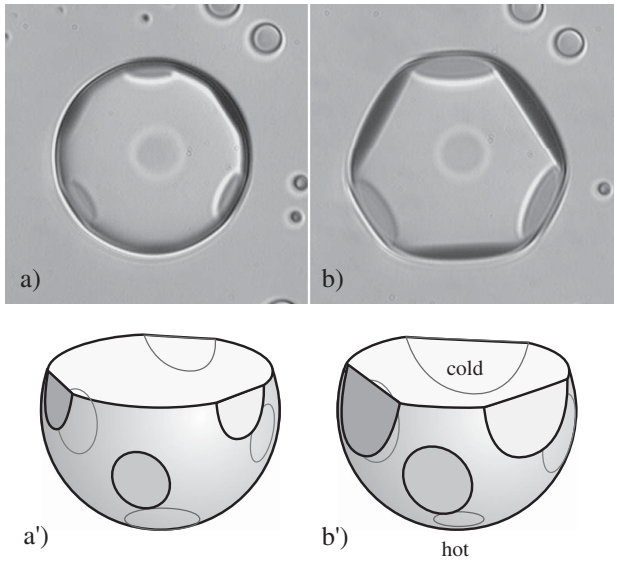

Figure 19. Deformation of a Pn3m crystal subjected to the vertical temperature gradient. Owing to the fact that the temperature gradient is parallel to the [111] axis of the crystal, the threefold symmetry of the crystal at uniform temperature (a) is preserved upon the temperature gradient (b). The perspective views in (a′) and (b′) emphasise that the crystallites are located at the upper wall of the capillary which is colder than the lower wall.

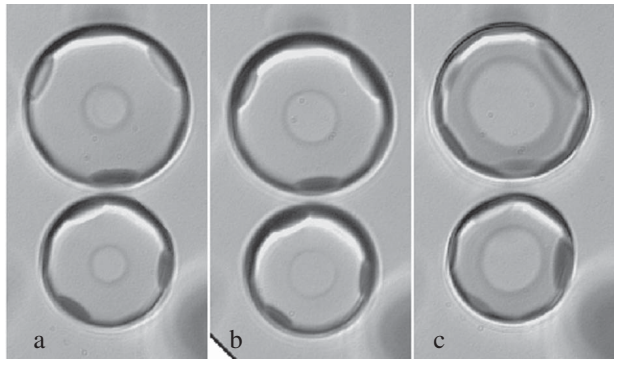

Figure 20. Deformation of a Pn3m crystal subjected to the vertical temperature gradient. The crystal sits now on the lower warmer wall of the capillary. In this reversed configuration, the central (111) facet is located now at the top of the crystal where the temperature is lower than at the bottom: (a) homogeneous temperature; (b) 1 hour after the application of the vertical temperature gradient; (c) 10 hours later.

The sign of the vertical temperature gradient with respect to the crystal can be reversed simply by flipping the flat capillary containing the sample upside-down. The series of three photographs in Figure 20 proves that in this reverse configuration, as expected, the central facet located now on the colder, upper side of the crystal becomes the largest.

2.3 L1-in-Pn3m inclusions, $C_{12}EO_2$/water binary system

When a temperature gradient parallel to the longitudinal axis of the glass capillary is applied, one observes a progressive deformation of L1 inclusions situated at capillary walls. In the example shown in Figure 21, the temperature gradient is 1 K mm^{-1}. This temperature gradient is applied to a system of three inclusions, the equilibrium shapes of which are shown in the photograph in the centre. The typical lateral size of these inclusions is 0.05 mm so that the temperature difference across them is of the order of 0.05 K. The two other photographs show the out-of-equilibrium shapes reached on the time scale of about 3 hours after the application of the temperature gradient. It is obvious from this example that the initial threefold symmetry is broken. Moreover, the modifications of the inclusions' shapes are similar to those of the crystals. The facets situated on the colder side of inclusions increase their size while those on the opposite side are shrinking.

2.4 Pn3m-in-L1 crystals, phytantriol/water/ethanol ternary system

2.4.1 On the necessity to work with a ternary system

As has been already mentioned in Section 1.2.2, bicontinuous cubic phases also occur in aqueous solutions

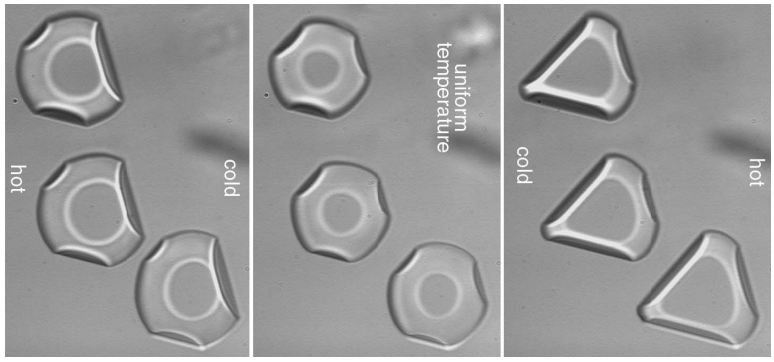

Figure 21. Deformation of L1 inclusions subjected to a temperature gradient. The temperature variation across one inclusion is of the order of 0.05 K.

of phytantriol. The phase diagram of phytantriol established by Barauskas and Landh (*22*) and shown here in Figure 22 displays the Pn3m/L1 phase coexistence, similarly to that of $C_{12}EO_2$ in Figure 10, yet with a much larger temperature range. This feature is an advantage for studies of the Ludwig–Soret effect. Unfortunately, the detailed structure of the phase diagram of phytantriol leads to a drawback from an experimental point of view. Indeed, in isoplethal experiments, owing to the presence of the Pn3m/H/L2 triple point, Pn3m-in-L1 crystals can only be grown from anisotropic hexagonal-in-L1 droplets. As a consequence, it is difficult to obtain well-shaped Pn3m-in-L1 monocrystals in contrast to the case of $C_{12}EO_2$ where Pn3m-in-L1 monocrystals were grown from isotropic L2-in-L1 or L3-in-L1 droplets (see Figure 10).

Stimulated by the method of Spicer and Hayden (*38*) of the preparation of cubosomes, we decided to check whether the hexagonal phase could be suppressed by the addition of ethanol to the water. Our experiments proved that this is actually true so that in the presence of ethanol, Pn3m-in-L1 crystals can be melted into L2-in-L1 droplets and subsequently recrystallised again as required. More precisely, in the ternary phytantriol/water/ethanol system, the Pn3m $\Longrightarrow$ L2 transition can be driven in two ways:

(1) by adding ethanol to the L1 phase surrounding crystals at constant temperature; or
(2) by increasing the temperature at a constant adequate concentration of ethanol in L1.

In both cases, the concentration of ethanol in the L1 phase has to be adjusted precisely. In practice, about 100 ml of the required solution of ethanol in water is first prepared and injected subsequently with a constant slow rate ($\approx 0.1\ \mu l\ s^{-1}$) into the capillary by means of a motorised syringe. As the phase diagram of the phytantriol/water/ethanol ternary system has not been established so far, in following we only specify the concentration of ethanol in the solution injected into the capillary. Let us stress that thanks to the continuous injection of a fresh solution, the concentration of ethanol in the L1 phase surrounding Pn3m crystals remains constant in spite of the Ludwig–Soret effect.

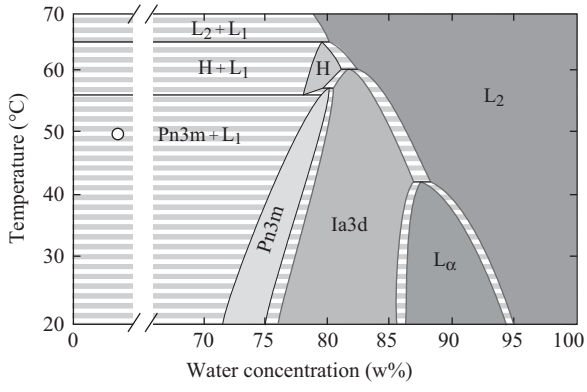

Figure 22. Phase diagram of the phytantriol/water binary system. (Modification of the phase diagram established by Barauskas and Landh (*22*). Made in collaboration with P. Faye and J. Okal.)

2.4.2 Deformation of Pn3m-in-L1 crystals in a horizontal temperature gradient

The series of six pictures in Figure 23(a) illustrates the evolution of a Pn3m-in-L1 crystal subjected to a horizontal temperature gradient of 2.4 K mm^{-1}. As in experiments with $C_{12}EO_2$/water system, the colder part of the crystal is growing and the warmer part is simultaneously deconstructed. Quantitative features of this behaviour can be obtained from the spatiotemporal cross-section shown in Figure 23(b). It has been extracted from a video by the reslice command along the axis *r* defined in Figure 23(a). In particular, it is obvious that:

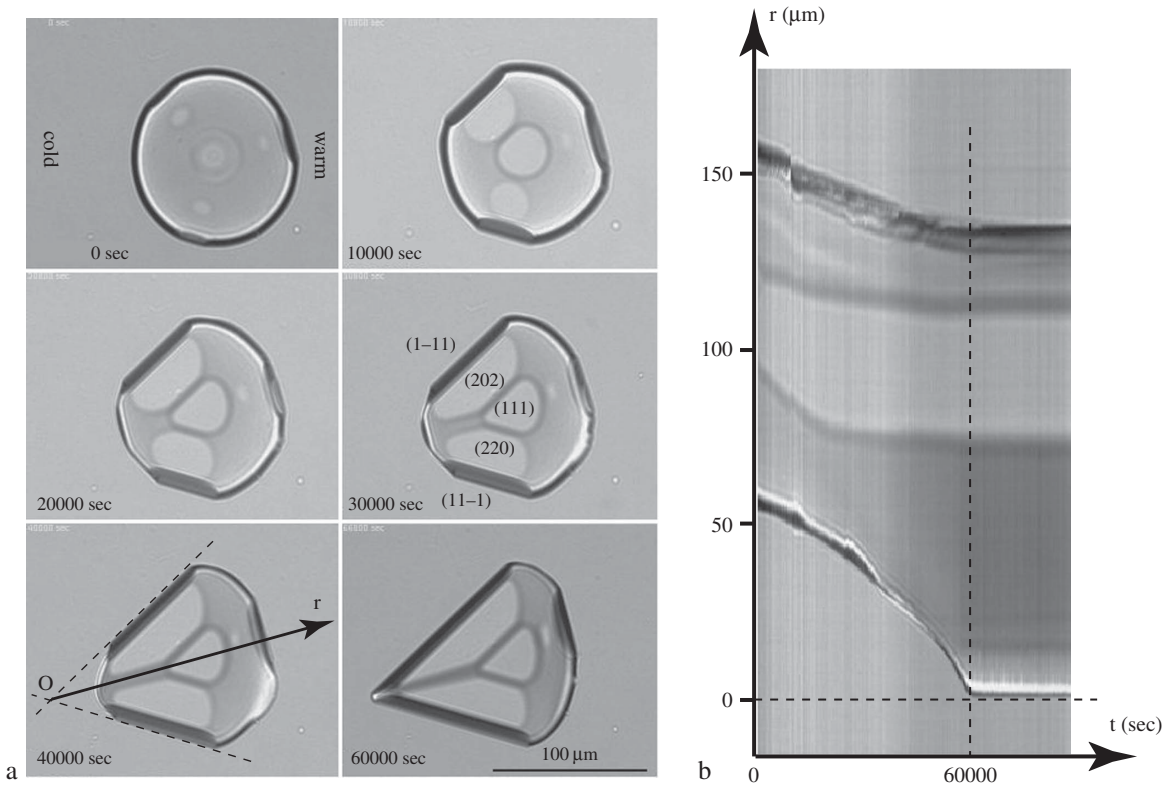

Figure 23. Deformation of Pn3m-in-L1 crystal subjected to a temperature gradient in the phytantriol/water/ethanol ternary system. The concentration of ethanol in the L1 phase is 4%. The temperature gradient is 2.4 K mm^{-1}. (a) Series of six images selected from a video. (b) Spatiotemporal section along the axis *r* defined in the picture labeled '40,000 sec', extracted from a video taken at a rate of 1 image per 400 seconds. (Made in collaboration with J. Rizzi and G. Saquet.)

(1) the velocity of the cold extremity of the crystal increases monotonically and suddenly falls to zero at time t_c = 60,000 seconds;
(2) this transition takes place when the facetting of the cold extremity is achieved i.e. when the mobile rough part of the crystal surface located between facets disappears;
(3) the velocity of the warmer extremity of the crystal decreases progressively and tends to zero at the same time t_c.

Let us also stress that the final sharp-pointed shape of the facetted cold extremity of the crystal in the last picture of Figure 23(a) is different from that in Figure 12(d). More precisely, only (111)-type facets are present on Pn3m crystals of $C_{12}EO_2$ while in the case of phytantriol (220)-type facets also occur. This difference is due to the phenomenon of the anisotropic surface melting discussed in (*32*). Owing to a very narrow temperature range of the Pn3m/L1 coexistence in $C_{12}EO_2$ phase diagram, facets other than (111) are melted. In the case of the phytantriol/water/ethanol ternary mixtures, (220), (400), (311) and (331) facets can also appear when temperature and/or ethanol concentration are lowered (see Section 1.3.1). The presence of these additional facets affects the evolution of crystal shapes. For example, in Figure 24 the cold extremity of the crystal is truncated by the (400) facet.

2.5 Im3m-in-L1 crystals, phytantriol/DSPG/water/ethanol quaternary system

To complete our study of the Ludwig–Soret effect in bicontinuous cubic phases we had to find a system in which the Im3m phase would coexist with the L1 phase. To the best of our knowledge, there are no binary systems having this property; however, it has been pointed our recently by Wadsten-Hindrichsen *et al.* (*23*) that the Pn3m phase is replaced by the Im3m phase when a small amount (less than 1 wt%) of DSPG (distearoylphospatidylglycerol) is added to the phytantriol. We have found that the Im3m/L1 phase coexistence persists when less than 14 wt% of ethanol is added to the L1 phase. Moreover, with 13 wt% of ethanol in L1, the Im3m $\leftrightarrows$ L3 phase transition occurs at $T = 34°C$ so that we were able to grow Im3m-in-L1 monocrystals. When such Im3m monocrystals

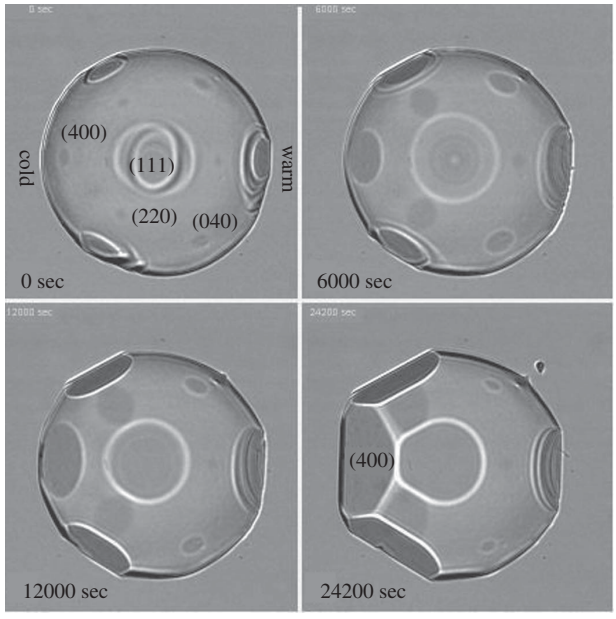

Figure 24. Deformation of Pn3m-in-L1 crystal subjected to a temperature gradient in the phytantriol/water/ethanol ternary system. The concentration of ethanol in the L1 phase is 4%. The temperature gradient is 2.4 K mm^{-1}. The average temperature of the crystal, 52°C, is lower than in Figure 23. As a consequence, the (400) facet truncates the cold extremity of the crystal. (Made in collaboration with J. Rizzi and G. Saquet.)

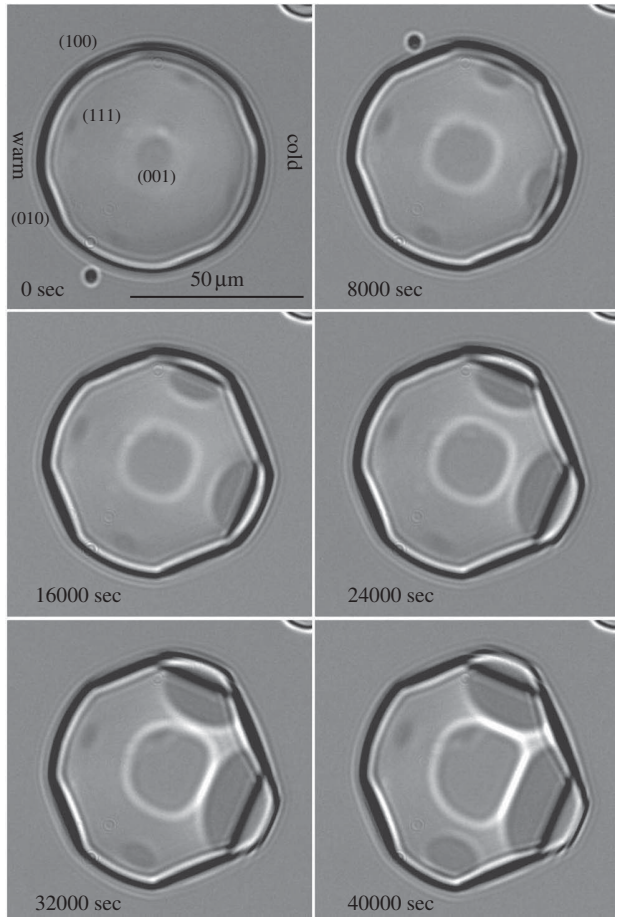

Figure 25. Phytantriol/DSPG/water/ethanol quaternary system. Deformation of a Im3m-in-L1 crystal subjected to a temperature gradient of 2 K mm^{-1}. The concentration of ethanol in L1 phase is 13%. The concentration of DSPG in phytantriol is less than 1%.

are subjected to a temperature gradient, they display the thermophobic Ludwig–Soret effect illustrated here by the series of six pictures in Figure 25.

3. Discussion

3.1 Experimental evidence for the transport of the surfactant by permeation through the unique triply periodic bilayer

Results of all experiments described in Section 2 lead to the conclusion that shapes of monocrystals of Ia3d, Pn3m and Im3m bicontinuous cubic phases are affected by temperature gradients in a similar way:

(1) cold extremities of the crystals are growing;
(2) the growth process involves only the outward motion of rough parts of the crystal surface; cold facets do not move but increase their size at the expense of the adjacent rough parts;
(3) warm extremities of the crystals are deconstructed;
(4) the deconstruction process involves a monotonic inward motion of rough parts of the crystal surface;
(5) warm facets are also moving but their inward motion is stepped since it results from successive generation of macroscopic steps on facets edges and collapse of these steps at the centre of the facets.

It is obvious that these growth and deconstruction processes involve transport of the surfactant from the warm to the cold extremities of crystals. In the case of Ia3d-in-vapour crystals, this transport cannot occur through the vapour phase because the $C_{12}EO_6$ surfactant is not volatile, i.e. its vapour pressure at room temperature is extremely low. In the case of Pn3m-in-L1 and Im3m-in-L1 crystals, the transport of surfactant cannot occur through the L1 phase either because the concentration of surfactants ($C_{12}EO_2$ or phytantriol) in it is negligible. We know this from the fact that the volume of Pn3m and Im3m crystals does not decrease on the time scale of months in spite of the fact that fresh water or fresh water/ethanol solution is permanently flowing around them. Moreover, if the surrounding solvent (L1 phase) was involved in the

transport of surfactant, the observed changes in crystal shapes would be affected by flow of the solvent which is not the case.

Therefore, we are left with the unique possibility of the transport of the surfactant through the crystal. We should even say 'transport of the surfactant through the lattice made of the unique bilayer', because the crystal lattice is at rest with respect to capillary walls; we know this from the fact that cold facets are at rest. This important conclusion is illustrated in Figure 26 by four drawings of the Pn3m level surface inside the crystal changing its shape (to be compared with Figure 23).

This kind of transport is similar to the permeation of molecules through smectic layers or through the cholesteric helix. Therefore, our final conclusion is that *temperature gradients drive the transport of surfactant by permeation, along triply periodic bilayers, from the warm toward the cold sides of crystals*.

The necessity of such a transport is also obvious in the case of the crystal having the unusual orientation with (110) planes parallel to the capillary wall shown in Figure 17. For the purpose of the theoretical analysis, we have represented this peculiar case schematically in Figure 27. By superposing the initial and final shapes of the crystal, it is obvious that the surfactant from the domain represented in white on the warm side of crystal has been transported by permeation through the bilayer toward the colder side of crystal where it is used for the growth of the domain represented in black.

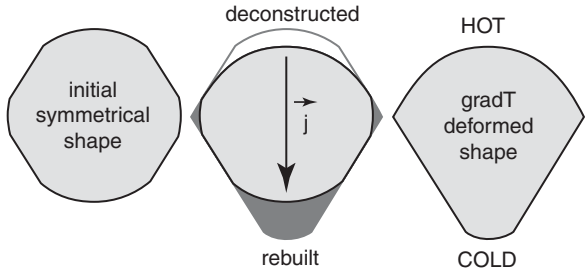

Figure 27. Transport of matter during the changes of crystal shapes induced by the horizontal temperature gradient (see Figure 17).

3.2 *Thermopermeation in lyotropic cubic phases*

Once the phenomenon of thermal diffusion of the surfactant *through bicontinuous cubic crystals* is established experimentally, we are ready to interpret it in terms of de Gennes' theory outlined in (*1*). To start with, we consider bicontinuous cubic crystals as porous media filled with water. We know already from Section 1.1.4 that the surface slip phenomenon and the geometry of pores play crucial roles in the theory of de Gennes. In cubic bicontinuous crystals, the geometry of pores is so complex that the nickname 'plumbers nightmare' was given to them. The case of Im3m crystal illustrated in Figure 28 is probably the easiest to apprehend. Here, the porous matrix is made of a unique surfactant bilayer separating two interwoven water labyrinths. Each labyrinth can be seen as a system of cavities interconnected by narrow channels. The cavities have roughly octahedral shapes and are located at sites of a simple cubic lattice. These cavities are connected by narrow channels running in x, y and z directions.

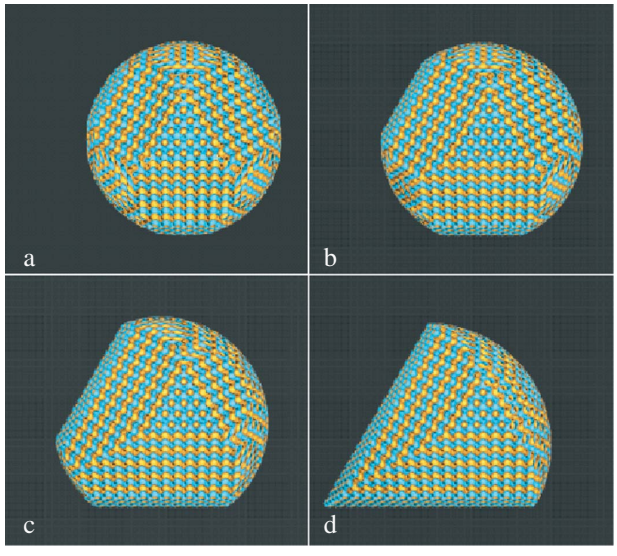

Figure 26. Simulation of the Soret effect in the Pn3m phase (see Figure 23).

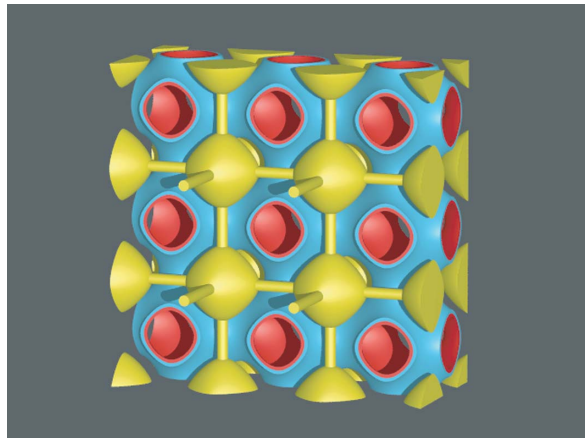

Figure 28. Approximate geometry of water channels in Im3m crystals. Only one of the two labyrinths is shown. The second labyrinth is identical and translated by $\mathbf{t} = (a/2, a/2, a/2)$ where a is the lattice constant.

3.2.1 Ansatz: solid elastic Im3m matrix

Let us suppose, for the time being, that the porous periodic matrix made of the unique surfactant bilayer behaves as a rigid solid. In such a case, the theory of de Gennes developed in (*1*) applies such as it is and tells us that the macroscopic flux density (per unit area) $\mathbf{j}_w$ of water through this *solid and porous* crystal is given by

$$\mathbf{j}_w = -\frac{k_w}{\eta_w}\nabla p_w - \overline{D}_{tw}\nabla T, \qquad (10)$$

where the two terms correspond respectively, to the Darcy law and to the thermal diffusion. Here, p_w is pressure in water, η_w is the viscosity of water, k_w is the permeability coefficient depending on the geometry of pores and $\overline{D}_{tw}$ is the thermal diffusion coefficient depending also on the geometry of the pores.

In the gedanken experiment imagined by de Gennes (see Figure 1(a)) and represented here once again in Figure 29(a), this current transfers water from the left to the right side of the crystal and a hydrostatic pressure difference Δp between the two sides of the crystal builds up. Owing to the growing contribution of the Darcy law term, the flux $\mathbf{j}_w$ decreases and tends to zero when the Darcy's term compensates exactly for the thermal diffusion's term. Let the pressure difference in this final hydrostatic state be $\Delta p = \Delta p_{\max}$.

Let us suppose now that the thermal gradient ∇T is suddenly suppressed. Owing to the pressure difference, water will flow through crystal's pores. In cylindrical channels connecting cavities, it will be a classical Poiseuille flow with a parabolic profile of the velocity field and the standard non-slip condition at the channels' walls, as shown in Figure 29(b). Such a Poiseuille flow exerts viscous stresses σ on the pores' walls.

In terms of de Gennes' theory, when the thermal gradient ∇T is switched on again, the slip $\mathbf{v}_{\text{slip}}$ in the direction opposite to the Poiseuille flow will occur at the channels' walls. The slip velocity is such that, for $\Delta p = \Delta p_{\max}$, the total flux through the channel is zero (see Figure 29(b′)). Note that the flow profile remains unchanged and the same stress σ acts on the pores' walls.

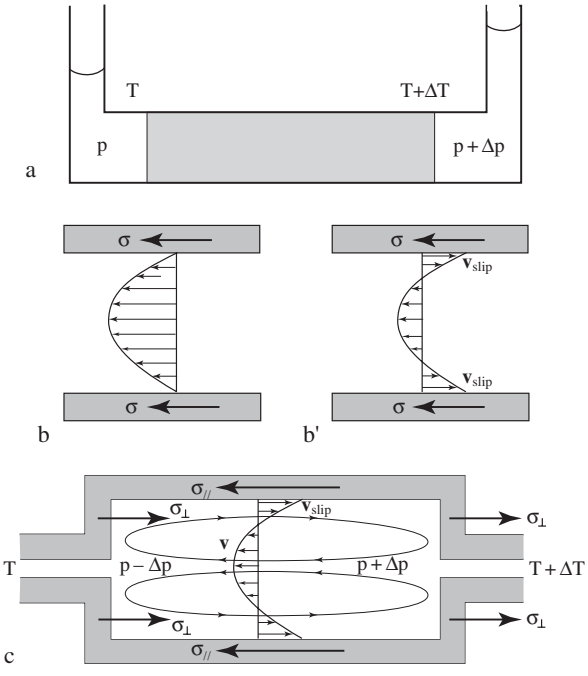

Figure 29. Flows and stresses in the gedanken experiment of de Gennes: (a) general view, similar to that in Figure 2(a); (b) flow profile when $\nabla T = 0$ and $\Delta p = \Delta p_{\max}$; (b′) flow profile when $\nabla T \neq 0$ and $\Delta p = \Delta p_{\max}$; (c) flow pattern in a channel of variable radius, $\nabla T \neq 0$.

3.2.2 Im3m matrix made of the surfactant bilayer

We are now ready to abandon the ansatz about the rock-solid nature of the Im3m matrix and to recall that in a real Im3m crystal, the porous matrix is made of the surfactant bilayer *which is liquid in its two dimensions*. The surfactant, subjected to the tangential stress σ, will flow inside the bilayer *in the direction opposite to* $\mathbf{v}_{\text{slip}}$. One could think that the mechanism of the surfactant transfer is found but we have to recall that the parabolic flow profile, which is necessary to generate the stress σ, is so far due to the pressure gradient driven from outside.

This is not the case in our experiments where Im3m crystals are surrounded by water so that they do not act as a dam and the pressure difference Δp cannot build up. Therefore, when the temperature gradient is switched on, the flow profile in narrow cylindrical channels is flat (plug flow) so that $\sigma = 0$ there and the mechanism of the surfactant transfer does not work.

We are left with the last possibility that surfactant flow could be generated by stresses acting on the walls of the large octahedral cavities. For the sake of simplicity, instead of octahedral, let us consider rather cylindrical elongated cavities, connected by much narrower cylindrical channels (see Figure 29(c)). Let us recall that we have already considered this configuration in Section 1.1.4. When the temperature gradient is switched on and the slip $\mathbf{v}_{\text{slip}}$ at lateral walls occurs, the necessary recirculation of water inside the cavity generates viscous shear stresses $\sigma_{\|}$ acting on the surfactant bilayer. Upon the action of these viscous stresses, the surfactant tends to flow inside the bilayer in the direction opposite to the slip of water.

Let us remark that if there was no external force acting on the cavity, the tangential viscous stresses $\sigma_{\parallel}$ could not exist alone. In fact, water flowing inside the cavity also exerts stresses $\sigma_{\perp}$ on cavity's walls due to variations $+\Delta p$ and $-\Delta p$ of the pressure p. Fortunately, in cubic bicontinuous crystals, these stresses *orthogonal to the bilayer* are balanced by the elastic response of the periodically curved bilayer in the crystal attached to the capillary wall.

In conclusion, the tangential viscous stresses, generated by water eddies in the cavities, will induce flows inside the bilayer and the surfactant will be transferred *through the crystal lattice* from the warm extremity of the crystal to the cold extremity.

3.2.3 *Laws of thermopermeation*

A detailed pattern of this flow inside the bilayer is certainly very complex because it involves viscous dissipation and some distribution of the two-dimensional pressure p_s. We do not tempt to solve this problem here. Let us just note that variation of the Gaussian curvature K along the Im3m periodic minimal surface is one possible dissipation source. Indeed, when, during the flow, a surface element of the bilayer is transported from point P to P' and $K(P) \neq K(P')$, then shear deformations occur in monolayers composing the bilayer and viscous dissipation is generated.

In the absence of knowledge of detailed microscopic mechanism, we can still write the phenomenological transport equation:

$$\mathbf{j}_s = -P_s \nabla p_s - D_{ts} \nabla T \tag{11}$$

relating the current of the surfactant $\mathbf{j}_s$ to gradients of pressure (inside the surfactant bilayer) and temperature. Here P_s is the permeation coefficient depending on the geometry of the bilayer and on the two-dimensional viscosity of the surfactant.

To this transport equation we have to add the equation of mass conservation as well as some appropriate boundary conditions. For example, considering that the concentration c of the surfactant inside the crystal is constant, one has

$$\operatorname{div} \mathbf{j}_s = 0. \tag{12}$$

Knowing that the cold facets are blocked, we have to assume that the flux component orthogonal to these facets is zero. If $\mathbf{m}_{hkl}$ is a normal to the facet (hkl), then one has

$$\mathbf{j}_s \cdot \mathbf{m}_{hkl} = 0. \tag{13}$$

On the other hand, the rough cold parts of the crystals surface can move and the velocity v of their progression is determined by the normal component of the flux:

$$\mathbf{j}_s \cdot \mathbf{m}_{\text{rough}} = cv. \tag{14}$$

3.3 *Evolution of crystal shapes in temperature gradients*

For the sake of simplicity in the search for analytical solutions of the set of Equations (11)–(14), it is necessary to make some suitable approximations of our experimental geometries. Let us consider, for example, the deformation of the Pn3m-in-L1 crystal shown in Figure 23. The growing cold extremity of the crystal, limited by the set of (111)-type and (220)-type facets, has a conical shape. Therefore, let us consider the idealised geometry shown in Figure 30 of a crystal confined into a cone and subjected to a radial temperature gradient $\partial T/\partial r = T_r$. In this geometry, the flux of the surfactant $\mathbf{j}_s$ has only the radial component; let us call it $\mathbf{j}_r$. Finally, $\mathbf{p}_s$ and $\mathbf{j}_r$, similarly to T, depend only on r.

In order to satisfy the incompressibility condition (12), the flux should be

$$j_r = \frac{C}{r^2}. \tag{15}$$

Therefore, the Equation (11) becomes:

$$\frac{C}{r^2} = -P_s \frac{\partial p_s}{\partial r} - D_{ts} T_r \tag{16}$$

and, after its integration, one obtains

$$P_s p_s(r) = \frac{C}{r} - D_{ts} T_r r + P_s p_0. \tag{17}$$

In order to find the two coefficients, C and p_0, we have to introduce the boundary conditions for pressures

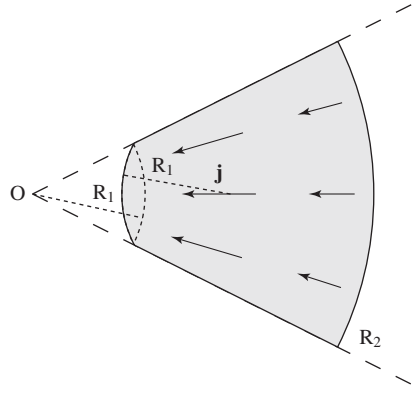

Figure 30. Simplified conical geometry.

$p_s(R_1)$ and $p_s(R_2)$ at the two interfaces which are free to move. One can for instance use the Laplace law and write

$$p_s(R_1) \approx \frac{\gamma}{R_1}, \tag{18}$$

$$p_s(R_2) \approx \frac{\gamma}{R_2}. \tag{19}$$

Using these boundary conditions, one obtains

$$C \approx -D_{ts}T_r R_1 R_2 + P_s\gamma. \tag{20}$$

During the evolution of the crystal shape, the two radii R_1 and R_2 remain related by the condition of the conservation of the crystal volume

$$V = \beta(R_2^3 - R_1^3). \tag{21}$$

Knowing C, we can now calculate, from (14), (15) and (21), fluxes (proportional to velocities $v = d\,R/dt$) at the cold and warm extremities of the crystal:

$$\begin{aligned} j_r(R_1) &= cv(R_1) \\ &= \frac{-D_{ts}T_r R_1 (V/\beta + R_1^3)^{1/3} + P_s\gamma}{R_1^2}, \end{aligned} \tag{22}$$

$$\begin{aligned} j_r(R_2) &= cv(R_2) \\ &= \frac{-D_{ts}T_r R_2 (R_2^3 - V/\beta)^{1/3} + P_s\gamma}{R_2^2}. \end{aligned} \tag{23}$$

In order to discuss the consequences of these equation it is useful to work with dimensionless variables $\tilde{r}$ and $\tilde{j}$ using

- $(V/\beta)^{1/3}$ as the length unit; and
- $D_{ts}T_r$ as the flux unit.

With an *a posteriori* justification, we also set

$$\frac{P_s\gamma}{D_{ts}T_r(V/\beta)^{1/3}} = 0.02 \tag{24}$$

and, finally, we obtain the dimensionless version of (22)

$$\tilde{j}_r(\tilde{R}_1) = \alpha\frac{d\tilde{R}_1}{dt} = \frac{-\tilde{R}_1(1 + \tilde{R}_1^3)^{1/3} + 0.02}{\tilde{R}_1^2} \tag{25}$$

with

$$\alpha = \frac{c(V/\beta)^{1/3}}{D_{ts}T_r}. \tag{26}$$

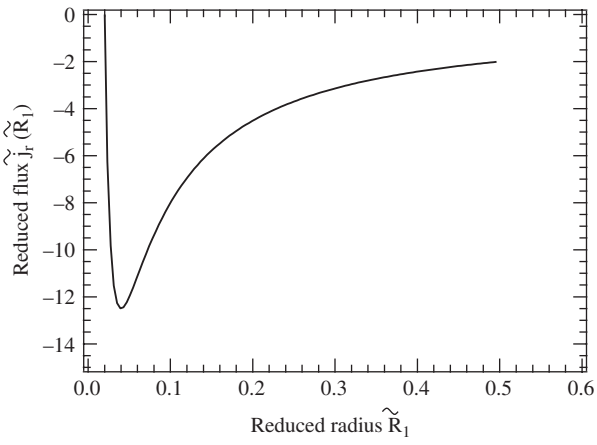

Figure 31. Reduced flux of the surfactant at the cold extremity of a conical crystal.

In Figure 31, we show how the reduced flux $\tilde{j}(\tilde{R}_1)$ (proportional to the velocity of the cold extremity of the crystal) depends on the reduced radius $\tilde{R}_1$. This velocity is negative which means that the cold extremity of the crystal moves toward the origin O (defined in Figure 30). This motion is faster and faster when $\tilde{R}_1$ varies from 0.5 to 0.04 because of the 'funnel' effect; the incompressible flux generated by thermopermeation has to pass through narrowing sections of the cone. Subsequently, for $\tilde{R}_1$, the adverse term of the Laplace pressure γ/R_1 starts to compete efficiently with the thermopermeation; the reduced flux $\tilde{j}_r(\tilde{R}_1)$ decreases with $\tilde{R}_1$ and tends to zero when the two terms are in balance.

Knowing that $\tilde{j}_r(\tilde{R}_1) = \alpha d\tilde{R}_1/dt$, we can use α as a unit of time and find how the reduced radius $\tilde{R}_1$ varies as a function of the reduced time $\tilde{t} = t/\alpha$ by integrating numerically (25) with respect to $\tilde{t}$. The result of this calculus is shown in Figure 32(a). Here, the second plot, $\tilde{R}_2(\tilde{t})$, is obtained from the relation $\tilde{R}_2^3 - \tilde{R}_1^3 = 1$.

In Figure 32(b), the two plots $\tilde{R}_1(\tilde{t})$ and $\tilde{R}_2(\tilde{t})$ are superposed with the spatiotemporal cross section from Figure 23(b). The plot $\tilde{R}_1(\tilde{t})$ fits well to the real motion of the cold extremity of the crystal. For the warm extremity, the agreement between our model and experiment is less satisfactory.

3.4 Structure of cubiclwater interfaces

The boundary conditions (18) and (19) at rough mobile surfaces of the Pn3m crystal play a crucial role for the evolution of its shape. In particular, the value of the dimensionless parameter α (proportional to the interfacial tension γ), determines the final shape of the crystal. Our choice of $\alpha = 0.02$ was based on the criterium of the best fit of the plot $\tilde{R}_1(\tilde{t})$ with the experimentally observed evolution of the cold extremity of the Pn3m crystal.

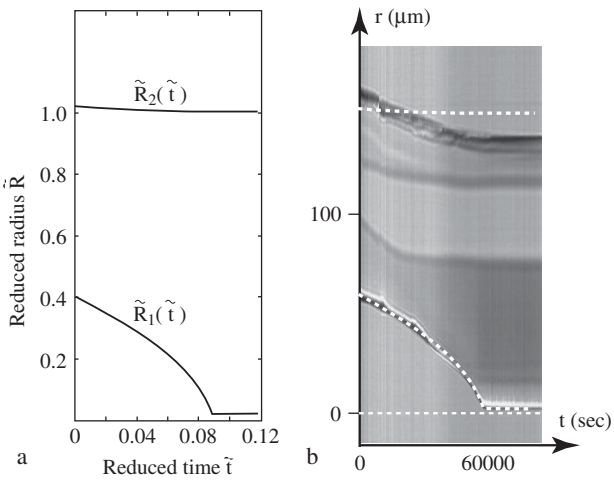

Figure 32. Motions of the cold and warm extremities of a conical crystal: (a) plots obtained by numerical integration of (25); (b) comparison with the experimental result from Figure 23(b).

Let us emphasise that, in addition to these *ad hoc* boundary conditions at the rough mobile parts of the Pn3m/L1 interface, the arrest of the crystal growth at (111)-type or (220)-type facets is also crucial for the evolution of crystal shapes.

These special boundary conditions at the facetted and rough parts of the Pn3m/L1 (Im3m/L1) interface lead to more general questions about structural details, energy cost and dynamics of the reconstruction of the bicontinuous Pn3m (Im3m) crystal at this interface.

One can ask, for instance, the following questions.

- Why are (100) and (111) types of facets the most stable on the Im3m/L1 interface while, on the Pn3m/L1 interface, it is the (111) and (220) types which are the most stable?
- What is the structure of these stable facets?
- What is the structure of the rough parts of the Pn3m/L1 (Im3m/L1) interface?
- How is the requirement of the continuity of the bilayer satisfied during the growth process on rough Pn3m/L1 (Im3m/L1) interfaces?

In the search for answers to these question, the method of cryotransmission electron microscopy is probably the most promising because it has been already used successfully for imaging cubosomes: monocrystals of cubic bicontinuous phases of submicrometre sizes (*39–44*).

4. Conclusions

The discovery of changes in shapes of lyotropic cubic crystals induced by temperature gradients was serendipitous. We observed this out-of-equilibrium effect for the first time during our studies of facetting of Ia3d-in-vapour crystals in a $C_{12}EO_6$/water system (*31*). Subsequently, we have found that the same effect occurs also in Pn3m-in-L1 and Im3m-in-L1 crystals of other binary, ternary and quaternary mixtures. Our findings were mentioned only very briefly in (*45*) and (*30*) while a more detailed description of experiments and their theoretical interpretation were waiting for publication in a separate article.

The kind invitation for contribution to the present issue of *Liquid Crystals* devoted to the memory of de Gennes accelerated the gathering of experimental results and triggered an elaboration of the theoretical model presented here.

The experiments presented in Section 2 consisted of observation, by means of an optical microscope, of the crystal shapes in three types of phase coexistence: Ia3d-in-vapour, Pn3m-in-L1 and Im3m-in-L1. In all three cases, we inferred from the evolution of crystal shapes that the surfactant is transferred, along the unique periodic bilayer, from the warm to the cold extremities of the crystals. We termed this phenomenon *thermopermeation* by etymological analogy with *thermophoresis* and *thermoosmosis*.

In its theoretical interpretation, we benefited from the ground broken by de Gennes in two apparently disjoined topics: (1) the Ludwig–Soret effect in porous media filled with pure liquids (*1*) and (2) bicontinuous structures in microemulsions (*2*). Indeed, in our model of thermopermeation, these two topics are now intimately related. Inspired by de Gennes, we postulated that:

- the periodic continuous bilayer made of surfactant is similar to the matrix of porous media;
- this matrix is elastic with respect to normal stresses;
- at the same time, it is liquid, in its two-dimensions, with respect to tangential stresses;
- thermal gradients generate a slip at the interface between this matrix and water (or water + ethanol) filling it.

A qualitative analysis of viscous stresses resulting from this slip led us to the conclusion that the surfactant should flow along the bilayer across the crystal lattice in the direction of thermal gradient. If this model gives a qualitative explanation of thermopermeation, it also raises several new questions about the structure of interfaces which have been already listed in the previous section.

Acknowledgements

This study of thermopermeation in lyotropic liquid crystal was exceptionally long (about 10 years) and as such it involved numerous collaborations, first of all, with students

who worked with me specifically on other topics: C. Even, D. Rohe, L. Sittler, M. Bouchih, N. Ginestet, S. Popa-Nita, T. Plötzing, J. Grenier, S. Leroy, J. Okal, P. Faye, R. Sheska, G. Saquet and J. Rizzi. Throughout this work, I also benefitted from interactions with experts in related topics. In particular, I had illuminating discussions with Paul Sotta, Vittorio Luzzati, Gregoire Porte and Christophe Blanc on the nature of bicontinuous phases and with Antonio Figueiredo Neto, Simone Wiegand, Roberto Piazza, Werner Köhler and Alois Würger on the Ludwig–Soret and related effects. I am also indebted for technical assistance to V. Klein, S. Saranga, D. Brunello, P.-J. Leroux, J.-L. Signoret, F. Quenault, J.-P. Dalac, Ch. Millien and C. Gendreau. This work was realised partially thanks to the financial support from BQR 'Étude physique des gouttes ou des films de cristaux liquides lyotropes placés sous humidité contrôlée'.

Last but not least, I would like to express my gratitude to P. G. de Gennes who always manifested his interest for my work and encouraged me to take the roads "less travelled by".

Note added in proof: After submission of this article the author has learnt that Reynolds (*46*) discovered thermophilic behaviour of gases in porous materials which has been termed "thermal transpiration" and this effect has been explained by Maxwell (*47*).

References

(1) de Gennes, P.-G. *C. R. Acad. Sci.* **1982**, *295*, 959–962.
(2) de Gennes, P.-G.; Taupin, C. *J. Phys. Chem.* **1982**, *86*, 2294–2304.
(3) Platten, J.K.; Costesèque, P. *Eur. Phys. J. E* **2004**, *15*, 235–239.
(4) Figueiredo Neto, A.M.; Salinas, R.S.A. *The Physics of Lyotropic Liquid Crystals*; Oxford University Press: Oxford, 2005; Chapter 8.
(5) Alves, S.; Demouchy, D.; Bee, A.; Talbots, D.; Bourdon, A.; Figueiredo Neto, A.M. *Phil. Mag.* **2003**, *83*, 2059–2066.
(6) Wittko, G.; Köhler, W. *Eur. Phys. J. E* **2006**, *21*, 283–291.
(7) Giglio, M.; Vendramini, A. *Phys. Rev. Lett.* **1977**, *38*, 26–30.
(8) Piazza, R.; Guarino A. *Phys. Rev. Lett.* **2002**, *63*, 208302.
(9) Ning, H.; Kita, R.; Kriegs, H.; Luettmer-Strathmann, J.; Wiegand, S. *J. Phys. Chem.* **2006**, *110*, 10746–10756.
(10) Piazza, R. *J. Phys.: Condens. Matter* **2004**, *16*, S4195–S4211.
(11) Würger, A. *Phys. Rev. Lett.* **2007**, *98*, 138301.
(12) Ruckenstein, E. *J. Coll. Interface Sci.* **1981**, *83*, 77.
(13) Scriven, L.E. Equilibrium Bicontinuous Structures. In *Micellazation, Solubilization and Microemulsions*, Mittal, K., Ed.; Plenum: New York, 1981, p. 877.
(14) Teubner, M. *Europhys. Lett.* **1991**, *14*, 403–408.
(15) Larsson, K. *Bicontinuous Liquid Crystals*; Surfactant Science Series 127, Lynch, M.L. and Spicer, P.T., Eds.; Taylor and Francis: London, 2005.
(16) Luzzati, V. et al. X-ray Diffraction Studies of Lipid–Water Systems. In *Biological Membranes,* Chapman, D., Ed.; Academic Press: New York, 1968.
(17) Larsson, K.; Fontell, K.; Krog N. *Chem. Phys. Lipids* **1980**, *27*, 321–328.
(18) Longley, W.; McIntosh, T.J. *Nature* **1983**, *303*, 612–614.
(19) Hyde, S.T.; Andersson, S.; Ericksson, B.; Larsson, K. *Z. Kristallogr.* **1984**, *168*, 213–219.
(20) Qiu, H.; Caffrey, M. *Biomaterials* **2000**, *21*, 223–234.
(21) Razumas, V.; Talaikite, Z.; Barauskas, J.; Larsson, K.; Miezis, Y.; Nylander, T. *Chem. Phys. Lipids* **1996**, *84*, 123–128.
(22) Barauskas, J.; Landh, T. *Langmuir* **2003**, *19*, 9562–9565.
(23) Wadsten-Hindirichsen, P.; Bender, J.; Unga, J.; Engström, S. *J. Coll. Interface. Sci.* **2007**, *315*, 701–713.
(24) Fontell, K. *Colloid Polym. Sci.* **1990**, *268*, 264–285.
(25) Schwarz, U.; Gompper, G. Bicontinuous Surfaces in Self-assembling Amphiphilic Systems. In *Morphology of Condensed Matter: Physics and Geometry of Spatially Complex Systems*; Lecture Notes in Physics 600, Mecke, K.R. and Stoyan, D., Eds.; Springer: Heidelberg, 2002, p. 107.
(26) Friedel, G. *Leçons de cristallographie*; Librairie Scientifique Albert Blachard: Paris, 1964.
(27) Phillips, F.C., *An Introduction to Crystallography*; Longmans: New York, 1960.
(28) Winsor, P.A. The influence of composition and temperature on the formation of mesophases in amphiphilic systems. The *R*-theory of fused micellar phases. In *Liquid Crystals and Plastic Crystals*, Vol. 1, Gray, G.W. and Winsor, P.A.; Ellis Horwood, 1974.
(29) Sotta, P.; *J. Physique II* **1983**, *1*, 763–772.
(30) Pieranski, P. *J. Phys.: Condens. Matter*, **2005**, *17*, S3333–S3339.
(31) Pieranski, P.; Sotta, P.; Rohe, D.; Imperor-Clerc, M. *Phys. Rev. Lett.* **2000**, *84*, 2409–2412.
(32) Leroy, S.; Grenier, J.; Rohe, D.; Even, C.; Pieranski, P. *Eur. Phys. J. E* **2006**, *20*, 19–27.
(33) Pieranski, P.; Bouchih, M.; Ginstet, N.; Popa-Nita, S. *Eur. Phys. J. E* **2003**, *12*, 239–254.
(34) Plötzing, T.; Pieranski, P. *Eur. Phys. J. E* **2004**, *13*, 179–188.
(35) Grenier, J.; Plötzing, T.; Rohe, D.; Pieranski, P. *Eur. Phys. J. E* **2006**, *19*, 223–232.
(36) Lynch, M.L.; Kochvar, K.A.; Burns, J.L.; Laughlin, R.G. *Langmuir* **2000**, *16*, 3537–3542.
(37) Popa-Nita, S. *Coexistence des phases lyotropes isotrope L1 and cubique Pn3m: formes des inclusions*, stage d'été, Laboratoire de Physique des Solides: Orsay, 2001
(38) Spicer, P.T.; Hayden, K.L. *Langmuir* **2001**, *17*, 5748–5756
(39) Gustafsson, J.; Ljusberg-Wahren, H.; Almgren, M.; Larsson, K. *Langmuir* **1996**, *12*, 4611–4613.
(40) Gustafsson, J.; Ljusberg-Wahren, H.; Almgren, M.; Larsson, K. *Langmuir* **1997**, *13*, 6964–6071.
(41) Spicer, P.T.; Hayden, K.L. *Langmuir* **2001**, *17*, 5748–5756.
(42) Yaghmur, A.; de Campo, L.; Segalowicz, L.; Leser, M.E.; Glatter, O. *Langmuir* **2005**, *21*, 569–577.
(43) Barauskas, J.; Johnsson, M.; Joabsson, F.; Tiberg, F. *Langmuir* **2005**, *21*, 2569–2577.
(44) Barauskas J.; Johnsson, M.; Tiberg, F. *Nanoletters* **2005**, *5*, 1615–1619.
(45) Pieranski, P.; Even, C.; Rohe, D.; Sittler, L.; Bouchih, M.; Ginestet, N.; Popa-Nita, S.; Plötzing, T.; Grenier, J. *Mol. Cryst. Liq. Cryst.* **2005**, *434*, 236.
(46) Reynolds, O., *Phil. Trans. R. Soc.* **1879**, *170*, 727–845.
(47) Maxwell, J.C., *Phil. Trans. R. Soc.* **1879**, *170*, 231–256.